Probing the N-Terminal β-Sheet Conversion in the Crystal Structure of the Human Prion Protein Bound to a Nanobody

Romany N. N. Abskharon,[†,‡,||,#] Gabriele Giachin,[§,#] Alexandre Wohlkonig,[†,‡,#] Sameh H. Soror,[†,‡,¶] Els Pardon,[†,‡] Giuseppe Legname,*,[§] and Jan Steyaert*,[†,‡]

[†]Structural Biology Brussels, Vrije Universiteit Brussel, Pleinlaan 2, 1050 Brussels, Belgium

[‡]Structural Biology Research Center, VIB, Pleinlaan 2, 1050 Brussels, Belgium

[||]National Institute of Oceanography and Fisheries (NIOF), 11516 Cairo, Egypt

[§]Department of Neuroscience, Laboratory of Prion Biology, Scuola Internazionale Superiore di Studi Avanzati (SISSA), 34136 Trieste, Italy

[¶]Center of Excellence, Helwan Structure Biology Research, Faculty of Pharmacy, Helwan University, 11795 Cairo, Egypt

S *Supporting Information*

ABSTRACT: Prions are fatal neurodegenerative transmissible agents causing several incurable illnesses in humans and animals. Prion diseases are caused by the structural conversion of the cellular prion protein, PrP^C, into its misfolded oligomeric form, known as prion or PrP^{Sc}. The canonical human PrP^C (HuPrP) fold features an unstructured N-terminal part (residues 23−124) and a well-defined C-terminal globular domain (residues 125−231). Compelling evidence indicates that an evolutionary N-terminal conserved motif AGAAAAGA (residues 113−120) plays an important role in the conversion to PrP^{Sc}. The intrinsic flexibility of the N-terminal has hampered efforts to obtain detailed atomic information on the structural features of this palindromic region. In this study, we crystallized the full-length HuPrP in complex with a nanobody (Nb484) that inhibits prion propagation. In the complex, the prion protein is unstructured from residue 23 to 116. The palindromic motif adopts a stable and fully extended configuration to form a three-stranded antiparallel β-sheet with the β1 and β2 strands, demonstrating that the full-length HuPrP^C can adopt a more elaborate β0-β1-α1-β2-α2-α3 structural organization than the canonical β1-α1-β2-α2-α3 prion-like fold. From this structure, it appears that the palindromic motif mediates β-enrichment in the PrP^C monomer as one of the early events in the conversion of PrP^C into PrP^{Sc}.
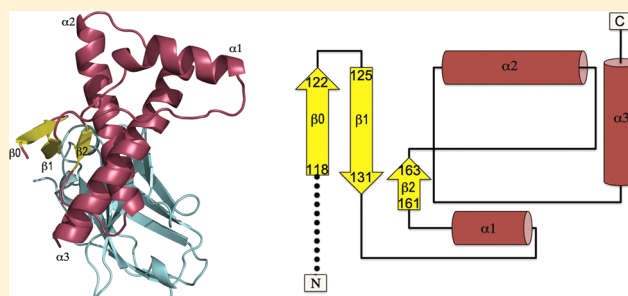
INTRODUCTION

The post-translational conversion of the ubiquitously expressed cellular form of the prion protein, PrP^C, into its misfolded oligomeric and pathogenic form, known as prion or PrP^{Sc}, plays a key role in prion diseases. These maladies are denoted transmissible spongiform encephalopathies (TSEs) and affect both humans and animals. TSEs can be sporadic, inherited, or infectious. In humans, sporadic Creutzfeldt−Jakob disease (CJD) is the most common prion malady.[1,2]

Structurally, PrP^C shows a very similar fold and amino acid sequence among different mammalian species. It is a glycosylphosphatidylinositol (GPI)-anchored glycoprotein featuring a long unstructured N-terminal part (from residue 23 to 124, hereinafter in human numbering) and a structured C-terminal domain (residues 125−231). The canonical PrP^C globular domain contains three α-helices (α1, α2, and α3) and two very short antiparallel β-strands (β1 and β2) folding into a characteristic β1-α1-β2-α2-α3 antiparallel beta-ribbon, referred to as the PrP^C-like fold in the Structural Classification of Proteins (SCOP) database.[3] A single disulfide bond bridges

helix α2 to α3.[4] The flexible N-terminal moiety contains functional subdomains that are able to coordinate the binding of divalent metal ions including a conserved octarepeat region (residues 60−91) as well as a positively charged segment (residues 96−111).[5] The ability of PrP^C to coordinate copper ions suggests it might also play a role in copper homeostasis. However, a unifying definition of PrP^C function has not yet been found. Therefore, PrP^C is often described as a pleiotropic protein involved in different physiological functions of neuronal and glial cells.[6]

Unlike that of PrP^C, the PrP^{Sc} structure contains significant β-sheet and few α-helix secondary motifs.[7,8] The structural features of PrP^{Sc} are responsible for its different physicochemical properties: while PrP^C is monomeric, soluble in nonionic detergents, and protease-K (PK) sensitive, PrP^{Sc} is insoluble, partially resistant to PK, and prone to aggregation. Limited digestion of PrP^{Sc} with PK produces an infectious fragment of

about 142 amino acids spanning approximately from residue 90 to 231, referred to as the PK-resistant core of PrP^{Sc}.[9] A prerequisite for understanding TSEs is unraveling the molecular mechanism leading to the structural conversion of PrP^C to prions. The insoluble and heterogeneous nature of PrP^{Sc} makes its structural characterization extremely difficult. Because of the lack of atomic details for PrP^{Sc}, different prion models have been proposed. One such model is based on fiber X-ray diffraction and imaging simulation techniques; it proposes that the segment ~90−175 forms a four-stranded β-sheet core organized in a β-helical configuration, whereas helices α2 and α3 retain their native conformation.[10] By contrast, hydrogen−deuterium exchange experiments on brain-derived PrP^{Sc} showed that the region from residue ~90 to the entire C-terminus displays slow exchange rates, which are typical for a structure comprising a continuum of β-strands.[11] The N-terminal of the PrP^{Sc} PK-resistant core features a palindromic sequence (AGAAAAGA), encompassing hydrophobic residues from 113 to 120, and it leads to the formation of neurotoxic fibrils enriched in β-sheet motifs.[12] Further experimental evidence supports the idea that the palindromic sequence plays a critical role for prion generation and transmissibility. In particular, in mature PrP^{Sc} this region is not accessible to antibodies recognizing this epitope in PrP^C, thus indicating that this segment undergoes conformational changes.[13] The ablation of only the palindromic sequence in transgenic mice[14] and murine neuroblastoma cells[15] is not toxic and seems to abrogate the conversion of the deletion mutant to PrP^{Sc}. Low-resolution spectroscopy data also indicate that the hydrophobic AGAAAAGA motif may adopt multiple discrete conformations; this might imply that this region is metastable and structures upon intermolecular interactions.[16,17] However, the intrinsic flexibility of this N-terminal has hampered efforts to obtain atomic information on the structural features of the palindromic region.

The solution structures of the full-length human prion protein, HuPrP(23−230), and two C-terminal fragments, HuPrP(90−230) and HuPrP(121−230), have been solved previously by NMR.[4] All these structures include a globular domain extending from residues 125−228 and an N-terminal flexibly disordered "tail." In this study, we used nanobodies to solve the very first structures of the full-length HuPrP (4KML.pdb) and its C-terminal truncated version (residues 90−231, 4N9O.pdb) by X-ray crystallography. Nb-assisted crystallography is a powerful tool to investigate the structure of target proteins that are difficult to crystallize because of their intrinsically disordered domains.[18−21] The high-resolution X-ray crystal structures of these HuPrPs in complex with a selective nanobody (Nb484) revealed a novel structural feature. While the segment from residue 128 to 225 shares a fold that is very similar to the corresponding NMR HuPrP structures, the binding of Nb484 to a region adjacent to the first β-sheet (β1) unveils key structural features of the hydrophobic segment from residue 117 to 128, which had remained unresolved in all the PrP structures published so far. In our X-ray structures, the sequence including the palindromic motif arranges in a novel β-strand we denoted as β0 (residues 118−122), which folds into a three-stranded antiparallel β-sheet with β1 and β2. The same structural arrangement was observed in both crystal structures, suggesting that it does not result from crystal packing but might have major biological implications for prion conversion. The implications of these findings are remarkable, as we provide a first atomic structural view of the palindromic region adopting a well-defined β-sheet conformation.

■ EXPERIMENTAL SECTION

Cloning, Expression, and Purification of Recombinant Prion Proteins. Open reading frames encoding HuPrP(23−231), HuPrP(90−231), MoPrP(23−230), or MoPrP(89−230) were cloned in the pET-28a vector (Novagen) as an Nde1-BamH1 fragment. HuPrP(23−231), HuPrP(90−231), MoPrP(23−230), or MoPrP(89−230) were expressed and purified as soluble proteins according to the literature.[22] HuPrP(23−144) was refolded from inclusion bodies according to the literature.[23,24]

Generation, Selection, and Purification of Anti-PrP Nanobodies. Two llamas were immunized 6 times biweekly with 200 μg of purified recombinant MoPrP(23−230) or MoPrP(89−230), respectively. Lymphocytes were collected from the anticoagulated blood of the immunized llamas to prepare a cDNA library of genes coding for the variable domains of the heavy-chain antibodies. Amplified PCR fragments were inserted into a pHEN4 phagemid vector and transformed in *E. coli* TG1 cells resulting in two separate phage-display libraries against recombinant MoPrP(23−230) or MoPrP(89−230), respectively. Both libraries contained at least 2 × 10^7 unique transformants with a VHH gene insert rate greater than 90%. The VHH libraries were displayed on phage following standard procedures,[25] and phage particles expressing MoPrP(23−230) or MoPrP(89−230) specific nanobodies were selected by panning on solid phase coated MoPrP(23−230) or MoPrP(89−230), respectively. Bound phages were recovered by incubating the antigen-coated wells with 100 mM triethylamine pH 10 for 10 min. Optionally, these MoPrP(23−230) or MoPrP(89−230) coated wells were neutralized with Tris-HCl pH 6.8 and washed several times with PBS after freshly grown TG1 cells were added to recover noneluted phage. For all the selections performed, a clear enrichment was observed after two to three consecutive rounds of panning. From each selection, 96 randomly chosen colonies from the second and third round of panning were grown to express the encoded Nb as a soluble protein. Crude periplasmic extracts were tested in ELISA against solid phase coated antigen. Positive clones were amplified by PCR and a *Hinf*I digestion was performed to analyze the diversity. Sequence analysis revealed 12 different sequence families against MoPrP(89−230) and two sequence families against MoPrP(23−230). All nanobodies were expressed and purified as previously described.[26]

Solid-Phase ELISA. Maxisorp 96-well plates (Nunc) were coated overnight at 4 °C with purified MoPrP(23−230) or MoPrP(89−230) at 2 μg/mL in sodium bicarbonate buffer pH 8.2. Residual protein binding sites in the wells were blocked with 2% milk in PBS for two hours at room temperature. Antigen-bound nanobodies were detected with a mouse anti-Hemagglutinin-alkaline phosphatase conjugated monoclonal antibody (clone 16B12, BAbCO) that binds the Hemagglutin in decapeptide-tag fused at the C-terminus of all nanobodies. Absorption at 405 nm was measured 20 min after adding the phosphatase substrate *p*-nitrophenyl phosphate.

Determination of Nb-PrP Affinities Using Surface Plasmon Resonance (SPR). Binding isotherms were determined on a Biacore 3000 (GE Healthcare). CM5 chips were activated with *N*-hydroxysuccinimide and *N*-ethyl-*N*-(3-dimethylaminopropyl) carbodiimide. For each PrP variant, 2 μg was diluted in 10 mM NaOAC at pH 5.2 and immobilized on the activated CM5 chip at a flow rate of 5 μL/min. Next, chips were blocked with ethanolamine. All binding and dissociation experiments were run at 30 μL/min flow rate in PBS, 0.05% Tween 20, and 3 mM EDTA at 25 °C. After each cycle, the surface was regenerated with a 60 s pulse of 100 mM glycine, pH 1.5. Association rates (K_{on}) and dissociation rates (K_{off}) were obtained using a simple 1:1 Langmuir binding model (Biacore evaluation software version 4.1). Equilibrium dissociation constant was calculated from the ratio K_{off}/K_{on}.

In Vitro Characterization of Nb484 in the Amyloid Seeding Assay. Amyloid seeding assays (ASA) were performed according to Colby et al., 2007 with minor modifications.[27] Briefly, a stock of 5 mg/mL of MoPrP(23−230) was diluted to 0.1 mg/mL (corresponding to
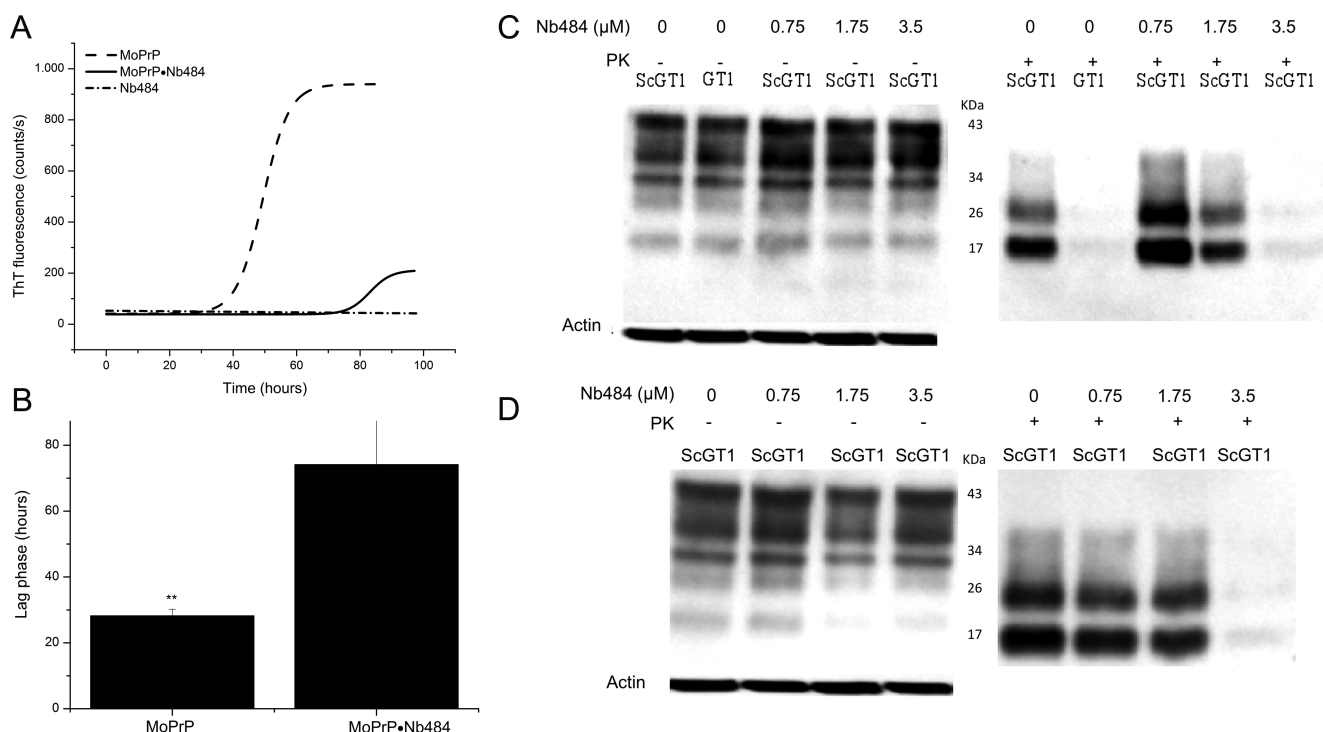
Figure 1. Nb484 inhibits prion propagation. (A) Amyloid seeding assay (ASA) to assess the fibrillization kinetics of the MoPrP(23−230)·Nb484 complex in the presence of preformed PrP^{Sc} seeds monitored by measuring the increase in ThT-fluorescence. Each curve is the average of four independent ASAs. Data were fitted to a sigmoidal Boltzmann curve. (B) Effect of Nb484 on the fibrillization lag phase (mean ± s.d., $N = 4$). Lag phases were estimated considering a 10% increase in the ThT fluorescence[28] (**$P < 0.01$). (C) Dose-dependent inhibition of PrP^{Sc} formation in ScGT1 cells treated with Nb484. After 7 days of culture in the presence of Nb484, cells were treated with protease-K (PK), and PrP^{Sc} levels were monitored by immunoblotting of lysed cells. (D) PrP^{Sc} levels in ScGT1 cells treated for 7 days with Nb484, followed by two 7-day passages in Nb-free medium.

4.3 μM) in PBS containing 0.4 M GndHCl, 10 mM Thioflavin T (ThT), preformed mouse PrP^{Sc} seeds, and nanobody. All ASAs were performed in a final volume of 200 μL in 96-well plate (BD Falcon, BD Bioscience). For agitation, each well contained one 3-mm glass bead (Sigma-Aldrich). Nb484 was added to each well at a final concentration of 5 μg/mL (corresponding to 0.3 μM). Our controls included wells containing only the seed in the presence or absence of Nb. Each condition was performed in four replicates. The plate was incubated at 37 °C with continuous shaking on a plate reader (Spectramax M5, Molecular Device). All seeds were purified from a hypothalamic ScGT1 murine cell line chronically infected by prions. Infected cells were lysed by adding 500 μL of PBS containing 4% sarkosyl, protease inhibitor (Complete, Roche), and 0.5% of the precipitant phosphotungstic acid (PTA) under continuous shaking (350 rpm) for 1 h at 37 °C. Seeds were recovered by centrifugation (14000g for 30 min), and pellets were washed, resuspended in lysis buffer, and then centrifuged again and resuspended in 150 μL of sterile double-distilled H$_2$O. Four μL of the resuspended PTA pellet was diluted in 400 μL of water, and 20 μL of this dilution was added to each well as the PrP^{Sc} seed. The kinetics of fibril formation was monitored by top reading of the fluorescence intensity every 5 min at 444 nm excitation and 485 nm emission. The lag phase was estimated on the basis of 10% of the ThT fluorescence increase.[28]

Treatment of ScGT1 Cells with Nb484. Scrapie-infected GT1 mouse hypothalamic (ScGT1) cells were seeded in 10-cm cell culture dish containing 10 mL of Dulbecco's modified Eagle's medium (DMEM) supplemented with 10% fetal bovine serum (FBS) and 1% penicillin−streptomycin. The cells were grown at 37 °C in 5% CO$_2$ to 95% confluence for 1 week before splitting at 1:10 for further cultivation. After splitting, cells were treated with increasing concentrations of Nb484 (0.75, 1.75, 3.5 μM) and incubated for 7 more days. After this treatment, the accumulation of PrP^{Sc} was detected by PK digestion followed by immunoblotting of lysed cells.

One mL of lysis buffer (10 mM Tris-HCl pH 8.0, 150 mM NaCl, 0.5% Nonidet P-40, 0.5% deoxycholic acid sodium salt) was added to the cell plates, and the cell lysates were collected after centrifugation at 1800g for 5 min. The total protein amount of the samples was measured by BCA (Pierce), and 250 μg of total protein was digested by PK (10 μg/mL) for 1 h at 37 °C. The reaction was stopped with 2 mM phenylmethylsulfonylfluoride (PMSF), and the PK-digested cell lysates were centrifuged at 150000g for 1 h at 4 °C in an ultracentrifuge (Beckman Coulter). The pellets were resuspended in 1× sample loading buffer. For the non-PK digested sample, 50 μg of cell lysates for ScGT1 was used and 2× loading buffer (125 mM Tris-HCl, pH 6.8, 10% 2-mercapethanol, 4% SDS, 0.2% bromophenol blue, 20% glycerol) was added in a 1:1 ratio. The samples were boiled for 5 min at 100 °C, loaded onto 15% Tris-Glycine SDS-PAGE gel, and transferred overnight onto Immobilon PVDF membranes (Millipore). Membranes were blocked by 5% nonfat milk, incubated with 1 μg/mL anti-PrP Fab D18 (InPro Biotechnology, South San Francisco, CA; ABR-0D18), followed by incubation with goat antihuman IgG F(ab)2 fragment conjugated with horseradish peroxidase. Blots were developed with the enhanced chemiluminescent system (ECL, Amersham Biosciences) and visualized on Hyperfilm (Amersham Biosciences). In another experiment, cells were incubated for 1 week in the presence of Nb484 as described above and next passaged twice for 7 days in Nb-free medium before they were lysed and analyzed for the presence of PrP^{Sc}.

Crystallization and Data Collection. Nb484 and HuPrP(23−231) or HuPrP(90−231) were mixed in an equimolar ratio to form protein complexes. Presence of a stable complex was monitored by analytical SEC using a Superdex 75 HR 10/30 column (GE Healthcare Life Sciences) using 20 mM Tris-HCl pH 7.5, 150 mM NaCl as the running buffer. HuPrP(23−231)·Nb484 crystals were grown at 20 °C in condition A9 of the MD-proplex screen (0.2 M sodium chloride, 0.1 M MES pH 6.0, 20% w/v PEG 2000 MME) at a final concentration of
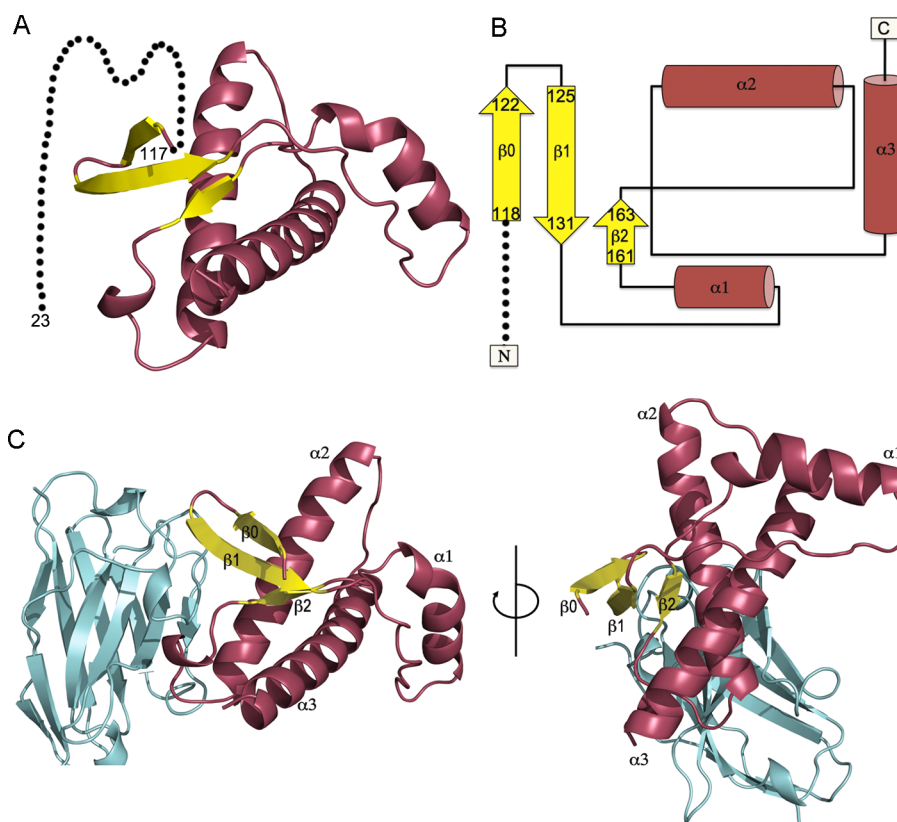
Figure 2. Crystal structure of the full-length HuPrP(23−231) in complex with Nb484. The structured part of full-length HuPrP is shown in crimson with the three-stranded antiparallel β-sheet highlighted in yellow. The nanobody is shown in cyan. (A) Cartoon representation of the HuPrP structure with the flexibly disordered "tail" of residues 23−116 represented by dots. (B) β0-β1-α1-β2-α2-α3 topology of HuPrP(23−231). (C) Ribbon representation of the complex shown in two orientations.

34 mg/mL. A high-resolution data set of 1.5 Å was collected at the X06DA beamline at SLS (Villigen, Switzerland). HuPrP(90−231)·Nb484 crystals were grown at 20 °C in condition F6 of MD-proplex screen (0.1 M HEPES-Na pH 7, 15% PEG20000) at a final concentration of 53 mg/mL within 3−4 weeks as described.[29] A high-resolution data set of 1.5 Å was collected on BM30 at the European Synchrotron Radiation Facility (ESRF, Grenoble, France). All crystals were cryoprotected using 15% glycerol.

Data Collection, Structure Determination, Refinement, and Model Building. Data were processed with XDS.[30] Table S1 (Supporting Information) summarizes the data collection details and refinement statics. The structures of the different HuPrP·Nb484 complexes were determined by molecular replacement (PHASER)[31] using the HuPrP crystal structure (pdb entry 2W9E)[32] and the structure of Nb484[26] as search models. Models were built manually using the Crystallographic Object-Oriented Toolkit (Coot),[33] and multiple refinement rounds were performed using Refmac5.[34] Structural analyses were performed using Ligplot,[35] Promotif,[36] DaliLite[37] or Pisa.[38]

RESULTS

Generation and Characterization of Nb484. Monoclonal antibodies with high affinity for PrP^C were generated as candidates for therapeutic approaches aimed to inhibit prion replication.[32,39,40] We selected 14 Nbs displaying high affinity for both human and mouse (Mo) PrPs (Table S2, Supporting Information). Nb484 displayed the highest affinity for HuPrP(23−231) and HuPrP(90−231) (Table S3, Figure S1, Supporting Information). To characterize Nb484 in the context of prion replication, we evaluated its effectiveness in inhibiting prion propagation using fibrillization and cell-based assays. We

assessed the fibrillization kinetics of the MoPrP(23−230)·Nb484 complex in the presence of a preformed PrP^{Sc} seed purified from ScGT1 cells. The addition of Nb484 to MoPrP(23−230) extended the lag phase of fibrillization by about 40 h in amyloid seeding assay (ASA).[27] This indicates that the interaction of Nb484 with the full-length MoPrP inhibits the formation of PrP^{Sc}-like aggregates (Figure 1A,B). To further confirm that Nb484 inhibits prion propagation, we treated scrapie infected murine cells (ScGT1) with different concentrations of Nb484. We evaluated the effect of the treatment measuring PrP^{Sc} level by PK assay and Western blotting. We observed that, compared with nontreated cells, the PrP^{Sc} levels in the ScGT1 cells treated with Nb484 were dramatically reduced in a dose-dependent manner. After adding 3.5 μM of Nb484, PrP^{Sc} levels were no longer detectable (Figure 1C). We also tested whether PrP^{Sc} remained undetectable after removing Nb484 from the medium. Cells previously treated with 3.5 μM of Nb484 exhibited PrP^{Sc} clearance upon its withdrawal (Figure 1D).

Nanobody-Assisted Crystallization of the Full-Length and Truncated HuPrPs. Atomic-level structural investigation of the events leading to conformational conversion of PrP^C to PrP^{Sc} has been challenging, because of the dynamic equilibrium among different structural species. The pathological process of amyloid formation observed in prion diseases usually takes several years in vivo, and the intermediate species are highly unstable. Using specific antibodies targeting proteins linked to neurodegenerative diseases (such as PrP^C, α-synuclein, or β-amyloid) may be a promising strategy for probing the amyloid formation process by biophysical methods including X-ray

crystallography.[41,42] We used Nb484 as crystallization chaperone to obtain high-resolution crystal structures of HuPrP(23−231) and HuPrP(90−231). Crystal structures were refined to 1.5 Å resolutions (Table S1, Supporting Information). Each cell unit was composed of a monomer of the HuPrP·Nb484 complex. Remarkably, clear electron density was available to confidently model half of the palindromic motif (residues 117−120) of both HuPrPs. The N-terminal downstream region remained highly unstructured in both crystals. We were able to refine the structure of the HuPrP from residues 117 to 225 and 118 to 224 for the full-length and truncated HuPrP, respectively. The average backbone root-mean-square distance between the refined structures is only 0.16 Å, indicating that both structures are identical. For clarity, hereinafter we will discuss the features of the HuPrP(23−231)·Nb484 complex. The segment from residue 128 to 225 of the HuPrP bound to Nb484 shares a fold that is very similar to that observed for the X-ray and NMR HuPrP structures (Figure S3, Supporting Information). HuPrP interacts with Nb484 through a discontinuous epitope including residues 123−125 in the β0-β1 loop, residues 164−170 in the β2-α2 loop, and residues 174−185 in the α2-helix. Table S4 (Supporting Information) shows a detailed overview of all the interactions between the folded domain of HuPrP and Nb484.

Remarkably, solving the full-length structure of the HuPrP using Nb-assisted crystallography revealed unprecedented structural features at the N-terminal palindromic sequence, which is close to the canonical fold. Although this segment has been reported as largely unfolded in several NMR HuPrP structures,[4,43,44] we identified the palindromic motif to be part of an extended three-stranded antiparallel β-sheet. This revealed a previously unresolved β-sheet secondary element (residues 118−122, denoted as β0) followed by two antiparallel β-strands comprising residues 125−131 (β1) and 161−163 (β2) (Figure 2). It thus appears that full-length HuPrP can adopt a more elaborate β0-β1-α1-β2-α2-α3 fold than the canonical prion-like β1-α1-β2-α2-α3 antiparallel beta-ribbon as defined in the SCOP classification.[3]

Structural Features of the Three-Stranded Antiparallel β-Sheet. While the hydrophobic region encompassing the conserved palindromic sequence has been reported as largely unfolded in all PrP structures, the palindromic motif is part of a previously unresolved three-stranded antiparallel β-sheet in the HuPrP(23−231)·Nb484 complex. In this structure, half of the palindromic sequence adopts a fully extended β-strand conformation (residues 118−122, denoted as β0) to pack against β1 followed by β2 (Figures 2A and S4, Supporting Information). Concomitantly, the β1 strand extends from the short three-residue strand (129−131) observed in all previous structures to a long seven-residue strand (125−131) that runs into a new well-structured loop between β0-β1 (Figure 2B). In this loop Gly123 and Gly124 occupy the i + 1 and i + 2 corner position of a type I′ β-turn[45] characterized by Phi-positive dihedral angles. The distance between the Cα atoms of residue i (Val122) and residue i + 3 (Leu125) is 5.5A. β0 and β1 form a 2:2 IP type β-hairpin. The tight I′ β-turn is stabilized by two cross-strand H-bonds involving Val122 and Leu125. Overall, β0, β1, and β2 form a canonical 3-stranded antiparallel β-sheet according to the conventions set by Kabsch and Sander.[45] Gly127 of β1 interrupts the regular hydrogen bonding network with β0 causing the elongated β1-strand to adopt a β-bulge motif[46] (Figures 3, S4, and S5, Supporting Information).
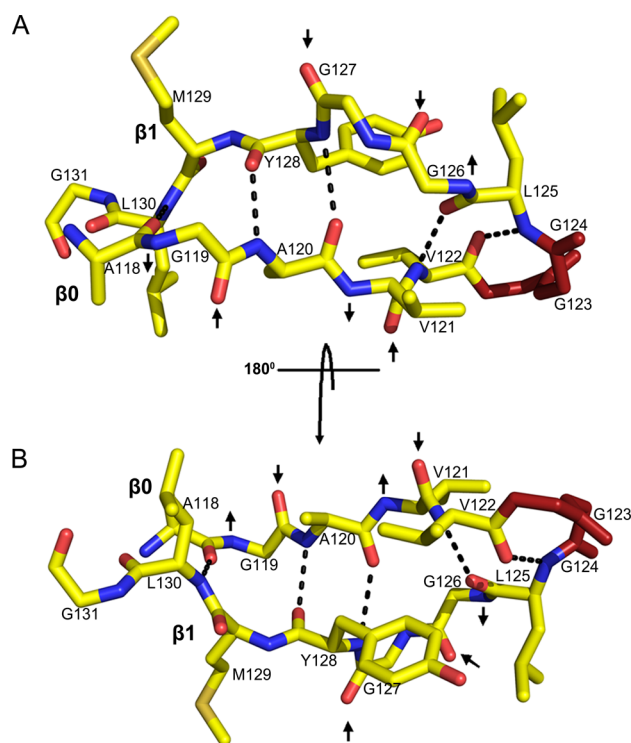

Figure 3. Structure of the β0-β1 hairpin in full-length HuPrP. The backbone donor and acceptor sites exposed to solvent are indicated by arrows. (A) Solvent-exposed face of the β0-β1 hairpin. (B) Solvent-protected face of the hairpin.

Stabilizing Interactions at the β2-α2 Loop and α2 Interfaces. The major HuPrP-Nb484 interacting surface includes a discontinuous C-terminal segment (residues 164−185) where the binding is stabilized by several H-bonds, salt-bridges, and aromatic interactions (Table S4, Figure S6, Supporting Information). The extensive contacts observed at the interface between the HuPrP C-terminal domain and Nb484 do not induce substantial local structural changes on this segment. The hydrophobic and aromatic interactions governing the proper folding of the β2-α2 loop and the α2-α3 helices are conserved like in other WT HuPrP X-ray and NMR structures. One important structural feature of the HuPrP· Nb484 complex is its significant stabilizing effect on the conformation of the β2-α2 loop region. This segment has been described as structurally flexible in all known HuPrP structures, but it is well-defined and rigid when bound to Nb484 (Figure S6, Supporting Information). This observed loop rigidity induced by Nb484 may have relevant biological implications. Indeed, different experimental studies proposed that the conformation of this loop plays a pivotal role in the development of TSEs.[47]

■ **DISCUSSION**

Elucidating the molecular mechanism that governs the PrP^C to PrP^Sc structural conversion is a central issue in prion biology. The misfolding of PrP^C to structures enriched in β-sheet is largely accepted as a determinant for neurotoxic signals triggered by PrP^Sc.[48] By different spectroscopic approaches, a series of seminal studies provided structural models of prion architectures.[10,11] However, the heterogeneous nature of PrP^Sc has so far eluded its detailed structural characterization. It has been postulated that the earliest event of the misfolding to

prions involves the formation of a metastable intermediate, denoted PrP*, which displays an aggregation-prone, β-sheet enriched structure.[49,50] Recent NMR studies on point mutations in HuPrP linked to genetic forms of human prion diseases[43,51,52] provided preliminary hints on the structural effect of the mutations clustered in the globular domain, but they have not yet clarified the structural rearrangements occurring at the N-terminal region, because of its flexibility. Here we used Nb-assisted crystallography as a strategy to obtain structural insights into HuPrP segments that are intrinsically disordered. In complex with the nanobody, the total amount of structured polypeptide (125 amino acids of antibody and 108 amino acids of HuPrP) rises to 71% as against 52% for free HuPrP, thus providing a much better starting point for crystallization. The nanobody contributes to generate a crystal lattice that leaves enough space for the N-terminal moiety (Figure S2, Supporting Information). The structure of the full-length HuPrP in complex with the nanobody reveals unprecedented structural features of the hydrophobic region encompassing the conserved palindromic sequence. This region first attracted interest because of its ability to form neurotoxic species[12,53] and inspired several in silico and in vitro studies, which characterized the structural properties of short peptides carrying the AGAAAAGA motif.[54−58]

The high resolution crystal structure of full-length HuPrP provides a first atomic structural view of the palindromic region adopting a well-defined β-sheet conformation. Edges of regular β-sheets are inherently aggregation-prone because the motif for H-bonding with any other β-strand is available.[59] From our structure, it appears that the exposed edge of the short β1 strand observed in all previous PrP structures serves as an intramolecular nucleus for edge-to-edge β aggregation of part of the palindromic sequence to form the β0 strand. The propensity of the palindromic sequence to engage in such β-structures strongly indicates that this motif mediates β-enrichment in the PrP^C monomer as one of the early events in the PrP^C to PrP^Sc conversion.

The observation that the conserved GGLGG sequence is contained in the β0-β1 hairpin may be particularly relevant to the structural conversion from PrP^C to PrP^Sc. GGX motives are common in fibrillogenic proteins like spider silk proteins.[60] The finding that Nb484 interacts with the GGLGG motif (Table S4, Supporting Information) is consistent with conversion mechanisms whereby the formation of the β0-β1 hairpin is facilitated either by intermolecular contacts with other PrPs or by yet unknown cellular cofactors. Possible concerns that the antibody has trapped the HuPrP in a non-native conformation are groundless. First, Nb484 does not interact with β0. More importantly, Nb484 is an in vivo matured conformational antibody that has been cloned from the blood of an immunized llama. In living animals, immature B cells expressing antibodies that have to pay a substantial energetic penalty for distorting the prion structure would not undergo clonal expansion to differentiate into mature B lymphocytes that circulate in the blood.[61]

At this stage it is still unclear how this early event of β-enrichment may drive a complete structural conversion of PrP^C to PrP^Sc. We found that the formation of the β0-β1 hairpin, including the GGLGG sequence, exposes several new backbone H-bond donor and acceptor sites to solvent (Figure 3). These sites are prone to stacking with other β-strands in a parallel or antiparallel configuration. Indeed, other strands may associate

perpendicularly to build large intermolecular β-sheets. It thus appears that the β-hairpin (β0-β1) can serve as a structural nucleus for the growth of intermolecular β-sheets. Remarkably, the hairpin configuration we observe in both structures also exposes to the solvent several hydrophobic side-chains including Ala118, Gly119, Val121, Gly126, and Gly127. This "dry surface" may provide a driving force for β-sheets of growing oligomers to associate and interdigitate to form steric zippers.[24]

The question remains: why is Nb484 able to halt prion replication in ScGT1 cells and in ASA acting as a molecular chaperone to stabilize PrP^C? Steric hindrance, whereby the antibody prevents the association of aggregation-prone metastable intermediates, may account for slowing down amyloidogenic conversion. Alternatively, conformational antibodies may prevent structural rearrangements that are pivotal for the formation of early intermediates. Nb484 binds and stabilizes a discontinuous epitope that includes the β2-α2 loop and half of the α2-helix (Figure S6, Table S4, Supporting Information). The b-factors indicate that the β2-α2 loop is significantly more rigid in the antibody complex as compared to PrP^C alone. The structural flexibility of this loop in PrP^C attracted particular interest in prion biology because it modulates the susceptibility of a given species to TSEs (Figure S7, Supporting Information). It has been observed that mammals (such as humans and mice) that express PrP with a flexible β2-α2 loop can be easily infected by prions, whereas species encoding PrP with a rigid loop (e.g., horse, rabbit, and marsupials)[62−64] do not develop spontaneous prion diseases under natural conditions. The structural stabilization of this critical epitope may represent an effective mechanism for Nb484 to inhibit prion formation.

Here we show that nanobody-assisted crystallography is a powerful tool to unveil local structural features of intrinsically disordered proteins. These data provide structural evidence that the palindromic motif is important as dynamic site for β-sheet structural conversion in prion formation. The structures we solved feed the hypothesis that the conserved palindromic sequence mediates β-enrichment in the PrP^C monomer as one of the early events in prion formation. Crystals of the full-length human PrP in complex with Nb484 are amenable to soaking experiments to study the interactions of small molecules with the flexible part of HuPrP.

■ ASSOCIATED CONTENT

Ⓢ Supporting Information

Details on the biophysical properties of the nanobodies, additional figures and tables, and tables of crystallographic data collection and refinement statistics. This material is available free of charge via the Internet at http://pubs.acs.org. The atomic coordinates have been deposited in the Protein Data Bank (PDB) with the following accession codes: 4KML and 4N9O.

■ AUTHOR INFORMATION

Corresponding Author

legname@sissa.it; jan.steyaert@vub.ac.be

Author Contributions

#R.N.N.A, G.G., and A.W. contributed equally.

Notes

The authors declare no competing financial interest.

REFERENCES

(1) Mastrianni, J. A. *Genet. Med.* **2010**, *12*, 187.

(2) Parchi, P.; Saverioni, D. *Folia Neuropathol.* **2012**, *50*, 20.

(3) Andreeva, A.; Howorth, D.; Chandonia, J. M.; Brenner, S. E.; Hubbard, T. J.; Chothia, C.; Murzin, A. G. *Nucleic Acids Res.* **2008**, *36*, D419.

(4) Zahn, R.; Liu, A.; Luhrs, T.; Riek, R.; von Schroetter, C.; Lopez Garcia, F.; Billeter, M.; Calzolai, L.; Wider, G.; Wuthrich, K. *Proc. Natl. Acad. Sci. U. S. A.* **2000**, *97*, 145.

(5) Walter, E. D.; Stevens, D. J.; Visconte, M. P.; Millhauser, G. L. *J. Am. Chem. Soc.* **2007**, *129*, 15440.

(6) Aguzzi, A.; Baumann, F.; Bremer, J. *Annu. Rev. Neurosci.* **2008**, *31*, 439.

(7) Gong, B.; Ramos, A.; Vazquez-Fernandez, E.; Silva, C. J.; Alonso, J.; Liu, Z.; Requena, J. R. *Biochemistry* **2011**, *50*, 4963.

(8) Pan, K. M.; Baldwin, M.; Nguyen, J.; Gasset, M.; Serban, A.; Groth, D.; Mehlhorn, I.; Huang, Z.; Fletterick, R. J.; Cohen, F. E.; et al. *Proc. Natl. Acad. Sci. U. S. A.* **1993**, *90*, 10962.

(9) Colby, D. W.; Prusiner, S. B. *Cold Spring Harbor Perspect. Biol.* **2011**, *3*, a006833.

(10) Wille, H.; Bian, W.; McDonald, M.; Kendall, A.; Colby, D. W.; Bloch, L.; Ollesch, J.; Borovinskiy, A. L.; Cohen, F. E.; Prusiner, S. B.; Stubbs, G. *Proc. Natl. Acad. Sci. U. S. A.* **2009**, *106*, 16990.

(11) Smirnovas, V.; Baron, G. S.; Offerdahl, D. K.; Raymond, G. J.; Caughey, B.; Surewicz, W. K. *Nat. Struct. Mol. Biol.* **2011**, *18*, 504.

(12) Forloni, G.; Angeretti, N.; Chiesa, R.; Monzani, E.; Salmona, M.; Bugiani, O.; Tagliavini, F. *Nature* **1993**, *362*, 543.

(13) Peretz, D.; Williamson, R. A.; Matsunaga, Y.; Serban, H.; Pinilla, C.; Bastidas, R. B.; Rozenshteyn, R.; James, T. L.; Houghten, R. A.; Cohen, F. E.; Prusiner, S. B.; Burton, D. R. *J. Mol. Biol.* **1997**, *273*, 614.

(14) Baumann, F.; Tolnay, M.; Brabeck, C.; Pahnke, J.; Kloz, U.; Niemann, H. H.; Heikenwalder, M.; Rulicke, T.; Burkle, A.; Aguzzi, A. *EMBO J.* **2007**, *26*, 538.

(15) Holscher, C.; Delius, H.; Burkle, A. *J. virol.* **1998**, *72*, 1153.

(16) Kuwata, K.; Matumoto, T.; Cheng, H.; Nagayama, K.; James, T. L.; Roder, H. *Proc. Natl. Acad. Sci. U. S. A.* **2003**, *100*, 14790.

(17) Lim, K. H.; Nguyen, T. N.; Damo, S. M.; Mazur, T.; Ball, H. L.; Prusiner, S. B.; Pines, A.; Wemmer, D. E. *Solid State Nucl. Magn. Reson.* **2006**, *29*, 183.

(18) De Genst, E. J.; Guilliams, T.; Wellens, J.; O'Day, E. M.; Waudby, C. A.; Meehan, S.; Dumoulin, M.; Hsu, S. T.; Cremades, N.; Verschueren, K. H.; Pardon, E.; Wyns, L.; Steyaert, J.; Christodoulou, J.; Dobson, C. M. *J. Mol. Biol.* **2010**, *402*, 326.

(19) Loris, R.; Marianovsky, I.; Lah, J.; Laeremans, T.; Engelberg-Kulka, H.; Glaser, G.; Muyldermans, S.; Wyns, L. *J. Biol. Chem.* **2003**, *278*, 28252.

(20) Rasmussen, S. G.; Choi, H. J.; Fung, J. J.; Pardon, E.; Casarosa, P.; Chae, P. S.; Devree, B. T.; Rosenbaum, D. M.; Thian, F. S.; Kobilka, T. S.; Schnapp, A.; Konetzki, I.; Sunahara, R. K.; Gellman, S. H.; Pautsch, A.; Steyaert, J.; Weis, W. I.; Kobilka, B. K. *Nature* **2011**, *469*, 175.

(21) Rasmussen, S. G.; DeVree, B. T.; Zou, Y.; Kruse, A. C.; Chung, K. Y.; Kobilka, T. S.; Thian, F. S.; Chae, P. S.; Pardon, E.; Calinski, D.; Mathiesen, J. M.; Shah, S. T.; Lyons, J. A.; Caffrey, M.; Gellman, S. H.; Steyaert, J.; Skiniotis, G.; Weis, W. I.; Sunahara, R. K.; Kobilka, B. K. *Nature* **2011**, *477*, 549.

(22) Abskharon, R. N.; Ramboarina, S.; El Hassan, H.; Gad, W.; Apostol, M. I.; Giachin, G.; Legname, G.; Steyaert, J.; Messens, J.; Soror, S. H.; Wohlkonig, A. *Microb. Cell Fact.* **2012**, *11*, 6.

(23) Zahn, R.; von Schroetter, C.; Wuthrich, K. *FEBS Lett.* **1997**, *417*, 400.

(24) Morillas, M.; Swietnicki, W.; Gambetti, P.; Surewicz, W. K. *J. Biol. Chem.* **1999**, *274*, 36859.

(25) Arbabi Ghahroudi, M.; Desmyter, A.; Wyns, L.; Hamers, R.; Muyldermans, S. *FEBS Lett.* **1997**, *414*, 521.

(26) Abskharon, R. N.; Soror, S. H.; Pardon, E.; El Hassan, H.; Legname, G.; Steyaert, J.; Wohlkonig, A. *Acta Crystallogr., Sect. F: Struct. Biol. Cryst. Commun.* **2010**, *66*, 1644.

(27) Colby, D. W.; Zhang, Q.; Wang, S.; Groth, D.; Legname, G.; Riesner, D.; Prusiner, S. B. *Proc. Natl. Acad. Sci. U. S. A.* **2007**, *104*, 20914.

(28) Polano, M.; Bek, A.; Benetti, F.; Lazzarino, M.; Legname, G. *J. Mol. Biol.* **2009**, *393*, 1033.

(29) Abskharon, R. N.; Soror, S. H.; Pardon, E.; El Hassan, H.; Legname, G.; Steyaert, J.; Wohlkonig, A. *Protein Eng., Des. Sel.* **2011**, *24*, 737.

(30) Kabsch, W. *Acta Crystallogr., Sect. D: Biol. Crystallogr.* **2010**, *66*, 133.

(31) McCoy, A. J. *Acta Crystallogr., Sect. D: Biol. Crystallogr.* **2007**, *63*, 32.

(32) Antonyuk, S. V.; Trevitt, C. R.; Strange, R. W.; Jackson, G. S.; Sangar, D.; Batchelor, M.; Cooper, S.; Fraser, C.; Jones, S.; Georgiou, T.; Khalili-Shirazi, A.; Clarke, A. R.; Hasnain, S. S.; Collinge, J. *Proc. Natl. Acad. Sci. U. S. A.* **2009**, *106*, 2554.

(33) Emsley, P.; Cowtan, K. *Acta Crystallogr., Sect. D: Biol. Crystallogr.* **2004**, *60*, 2126.

(34) Vagin, A. A.; Steiner, R. A.; Lebedev, A. A.; Potterton, L.; McNicholas, S.; Long, F.; Murshudov, G. N. *Acta Crystallogr., Sect. D: Biol. Crystallogr.* **2004**, *60*, 2184.

(35) Wallace, A. C.; Laskowski, R. A.; Thornton, J. M. *Protein Eng.* **1995**, *8*, 127.

(36) Hutchinson, E. G.; Thornton, J. M. *Protein Sci.* **1996**, *5*, 212.

(37) Dietmann, S.; Park, J.; Notredame, C.; Heger, A.; Lappe, M.; Holm, L. *Nucleic Acids Res.* **2001**, *29*, 55.

(38) Krissinel, E.; Henrick, K. *J. Mol. Biol.* **2007**, *372*, 774.

(39) Jones, D. R.; Taylor, W. A.; Bate, C.; David, M.; Tayebi, M. *PLoS One* **2010**, *5*, e9804.

(40) Peretz, D.; Williamson, R. A.; Kaneko, K.; Vergara, J.; Leclerc, E.; Schmitt-Ulms, G.; Mehlhorn, I. R.; Legname, G.; Wormald, M. R.; Rudd, P. M.; Dwek, R. A.; Burton, D. R.; Prusiner, S. B. *Nature* **2001**, *412*, 739.

(41) Domanska, K.; Vanderhaegen, S.; Srinivasan, V.; Pardon, E.; Dupeux, F.; Marquez, J. A.; Giorgetti, S.; Stoppini, M.; Wyns, L.; Bellotti, V.; Steyaert, J. *Proc. Natl. Acad. Sci. U. S. A.* **2011**, *108*, 1314.

(42) Dumoulin, M.; Dobson, C. M. *Biochimie* **2004**, *86*, 589.

(43) Biljan, I.; Ilc, G.; Giachin, G.; Plavec, J.; Legname, G. *Biochemistry* **2012**, *51*, 7465.

(44) Calzolai, L.; Zahn, R. *J. Biol. Chem.* **2003**, *278*, 35592.

(45) Venkatachalam, C. M. *Biopolymers* **1968**, *6*, 1425.

(46) Chan, A. W.; Hutchinson, E. G.; Harris, D.; Thornton, J. M. *Protein Sci.* **1993**, *2*, 1574.

(47) Sigurdson, C. J.; Nilsson, K. P.; Hornemann, S.; Manco, G.; Fernandez-Borges, N.; Schwarz, P.; Castilla, J.; Wuthrich, K.; Aguzzi, A. *J. Clin. Invest.* **2010**, *120*, 2590.

(48) Aguzzi, A.; Falsig, J. *Nat. Neurosci.* **2012**, *15*, 936.

(49) Khan, M. Q.; Sweeting, B.; Mulligan, V. K.; Arslan, P. E.; Cashman, N. R.; Pai, E. F.; Chakrabartty, A. *Proc. Natl. Acad. Sci. U. S. A.* **2010**, *107*, 19808.

(50) Kuwata, K.; Li, H.; Yamada, H.; Legname, G.; Prusiner, S. B.; Akasaka, K.; James, T. L. *Biochemistry* **2002**, *41*, 12277.

(51) Biljan, I.; Ilc, G.; Giachin, G.; Raspadori, A.; Zhukov, I.; Plavec, J.; Legname, G. *J. Mol. Biol.* **2011**, *412*, 660.

(52) Ilc, G.; Giachin, G.; Jaremko, M.; Jaremko, L.; Benetti, F.; Plavec, J.; Zhukov, I.; Legname, G. *PLoS One* **2010**, *5*, e11715.

(53) Jobling, M. F.; Stewart, L. R.; White, A. R.; McLean, C.; Friedhuber, A.; Maher, F.; Beyreuther, K.; Masters, C. L.; Barrow, C. J.; Collins, S. J.; Cappai, R. *J. Neurochem.* **1999**, *73*, 1557.

(54) Walsh, P.; Neudecker, P.; Sharpe, S. *J. Am. Chem. Soc.* **2010**, *132*, 7684.

943

dx.doi.org/10.1021/ja407527p | *J. Am. Chem. Soc.* 2014, 136, 937−944

(55) Cheng, H. M.; Tsai, T. W.; Huang, W. Y.; Lee, H. K.; Lian, H. Y.; Chou, F. C.; Mou, Y.; Chan, J. C. *Biochemistry* **2011**, *50*, 6815.

(56) Norstrom, E. M.; Mastrianni, J. A. *J. Biol. Chem.* **2005**, *280*, 27236.

(57) Silva, R. A.; Barber-Armstrong, W.; Decatur, S. M. *J. Am. Chem. Soc.* **2003**, *125*, 13674.

(58) Lee, S. W.; Mou, Y.; Lin, S. Y.; Chou, F. C.; Tseng, W. H.; Chen, C. H.; Lu, C. Y.; Yu, S. S.; Chan, J. C. *J. Mol. Biol.* **2008**, *378*, 1142.

(59) Richardson, J. S.; Richardson, D. C. *Proc. Natl. Acad. Sci. U. S. A.* **2002**, *99*, 2754.

(60) Gatesy, J.; Hayashi, C.; Motriuk, D.; Woods, J.; Lewis, R. *Science* **2001**, *291*, 2603.

(61) Steyaert, J.; Kobilka, B. K. *Curr. Opin. Struct. Biol.* **2011**, *21*, 567.

(62) Wen, Y.; Li, J.; Yao, W.; Xiong, M.; Hong, J.; Peng, Y.; Xiao, G.; Lin, D. *J. Biol. Chem.* **2010**, *285*, 31682.

(63) Christen, B.; Hornemann, S.; Damberger, F. F.; Wuthrich, K. *J. Mol. Biol.* **2009**, *389*, 833.

(64) Perez, D. R.; Damberger, F. F.; Wuthrich, K. *J. Mol. Biol.* **2010**, *400*, 121.

944

dx.doi.org/10.1021/ja407527p | *J. Am. Chem. Soc.* 2014, 136, 937−944